Journal of Medical Systems (2019) 43:331
https://doi.org/10.1007/s10916-019-1464-5

IMAGE & SIGNAL PROCESSING

Prediction of Clinical Pathologic Prognostic Factors for Rectal Adenocarcinoma: Volumetric Texture Analysis Based on Apparent Diffusion Coefficient Maps

Zhihua Lu[1] · Lei Wang[1] · Kaijian Xia[1] · Heng Jiang[1] · Xiaoyan Weng[1] · Jianlong Jiang[1] · Mei Wu[1]

Received: 23 April 2019 / Accepted: 26 September 2019

Abstract
Texture analysis has been used to characterize and measure tissue heterogeneity in medical images. The purpose of this study was to investigate the potential of texture features derived from apparent diffusion coefficient (ADC) maps, to serve as imaging markers for predicting important histopathologic prognostic factors in rectal cancer. One hundred patients of rectal cancer received 3 T preoperative magnetic resonance imaging including diffusion-weighted imaging (DWI). Skewness, kurtosis, uniformity from the histogram and entropy, energy, inertia, correlation from gray-level co-occurrence matrix (GLCM) derived from whole-lesion volumes were measured. Independent sample *t*-test or Mann-Whitney *U*-test and receiver operating characteristic (ROC) curves were used for statistical analysis. Uniformity, energy and entropy were significantly different ($p = 0.026$, 0.001, and 0.006, respectively) between stage pT1–2 and pT3–4 tumors. Skewness, kurtosis and correlation were significantly different ($p = 0.000$, 0.006, and 0.041, respectively) between grade 1–2 and grade 3 tumors. Energy and entropy ($p = 0.008$ and 0.033, respectively) could significantly differentiate negative circumferential resection margin (CRM) from positive CRM. Furthermore, predicted probabilities derived by logistic regression analysis yielded greater area under the curve (AUC) in differentiating pT3–4 stage and grade 3 grade tumors. Texture features derived from ADC maps may useful to predict important histopathologic prognostic factors of rectal cancer.

Keywords Diffusion-weighted imaging · Apparent diffusion coefficient · Rectal cancer · Texture analysis

Background

The prognosis of patients with rectal adenocarcinoma depends on many factors, some of which are evaluated by histopathology of surgical specimens. These factors include the depth that tumor extended into or beyond muscularis propria, number of lymph nodes affected by tumor spreading, tumor differentiation grade, invasion of the circumferential resection margin (CRM) [1–3] and peritumor lymphangiovascular invasion (LVI) or neural invasion [4, 5]. Other factors with proven prognostic importance include the plasma carcinoembryonic antigen (CEA) level [2]. Therefore, an accurate preoperative assessment of rectal adenocarcinoma is of great importance because the treatment strategies need to be individualized according to histopathological results.

Diffusion-weighted imaging (DWI) is a functional imaging technique of magnetic resonance imaging (MRI) that detects different movement of water protons in the extracellular to discriminate different tissues of cellular morphology [6]. In oncology, heterogeneity in cellular morphology can be investigated using DWI. Therefore, apparent diffusion coefficient (ADC) estimated from DWI has become a valuable image biomarker for tumor aggressiveness during past 10 years [7–12]. However, mean or median values are always not sufficiently sensitive to small changes or precise status of the tumor due to the intrinsic chaotic environment of tumors [13].

Texture analysis (TA) is a mathematical-statistical procedure to extract texture features by evaluating the spatial variation of gray levels within given images [14]. In recent years, TA has been used to characterize and measure tissue

This article is part of the Topical Collection on *Image & Signal Processing*

Zhihua Lu and Lei Wang are co-first authors.

✉ Zhihua Lu
luzhihua79@163.com

[1] First People's Hospital of Changshu City, Changshu Hospital Affiliated to Soochow University, Changshu, Jiangsu, China

Published online: 07 November 2019

heterogeneity in medical images. Compared with visual assessment, computational TA is more objective and more sensitive to detect subtle, sub-resolution changes in tumor morphology-changes [15–17]. Some texture features derived from MRI or computed tomography (CT) have been shown to be useful tools for accurate diagnosis, preoperative risk stratification, and assessment of treatment response in several cancers. For example, skewness and kurtosis differed significantly in cervical cancer with pelvic lymph node metastasis positive versus negative [15]. Haralick-based texture features showed useful to differentiate between non-cancerous and cancerous prostate gland [18]. In endometrial cancer, MR-derived tumor texture parameters were associated with the positive invasion of deep myometrial, lymphovascular space, and high-grade tumor [19, 20].

Due to the DWI is increasingly incorporated into rectal cancer imaging protocols, we speculated that texture features derived from an ADC map could predict important histopathological prognostic factors and thus possibly improve individualized treatment planning. The aim of this work was to evaluate the association between ADC map-derived texture features and prognostic factors of rectal adenocarcinoma.

Methods

Patients

This prospective study was approved by the Institutional Review Board of Changshu Hospital of Soochow University. Requirements for written informed consent were waived due to the retrospective nature of the study. Between October 2016 and October 2018, the records of 114 consecutive patients who had undergone rectal MRI for suspected rectal cancer were reviewed. Selection criteria included: (1) histological biopsy of proven rectal adenocarcinoma, (2) treatment by surgical resection without neoadjuvant therapy, (3) available pathological reports of surgical specimens. Fourteen patients were excluded for the following reasons: (1) image quality of DWI is poor ($n = 4$), (2) not having treatment by surgical resection in our hospital ($n = 6$), (3) having another type of pathology, such as mucinous adenocarcinoma (n = 4). Finally, the study population consisted of 100 patients (56 men, 44 women), with a median age of 68.5 years (range, 41–89 years).

MRI Techniques

All patients were imaged with a 3-T MRI system (InteraAchieva 3.0 T TX, Philips Medical System, Best, The Netherlands) using a 16-channel phased-array surface coil. Thirty minutes before MR examination, all patients were asked to take clyster in order to reduce artifacts induced by gas within the rectum. Patients received 10 mg of anisodamine (Hangzhou Mingsheng Pharmaceuticals Co., Ltd.) by intramuscular injection 10 min before the examination to reduce bowel peristalsis.

The standard rectal imaging protocol consisted of T2 weighted image (T2WI), DWI, and dynamic contrast-enhanced MR. T2WI included routine sagittal fast spin-echo (FSE) T2WI and high-resolution axial and coronal T2WI (Table 1). DWI was acquired with a single-shot spin echo planar imaging in axial orientation using the following b-values: 0 and 1000 s/mm^2. Dynamic contrast enhanced imaging was not assessed in this study.

Image Analysis and Textural Features Calculation

ADC maps were automatically computed from the DWI using a mono-exponential decay model. The whole-lesion analysis was performed independently by two radiologists (Zhihua Lu and Heng Jiang, with 8 and 4 years of experience reviewing rectal MRI, respectively) based on final pathological outcomes. The primary tumor site was determined as a focal mass or abnormal wall thickening that had intermediate intensity of signal on T2WI, hyperintensity on DWI and corresponding hypointensity on gray scale ADC map. The ADC maps were imported into our in-house software (Omni-Kinetics, GE Healthcare) for segmentation of regions of interest (ROI) and TA. ROIs were manually drawn slice by slice, just inside the outer margin of the lesion to minimize partial volume error, to cover as much of the entire tumor area as possible on ADC maps with reference of T2WI and DWI. The areas of necrosis, cysts, and gas were avoided to minimize bias. All the ROIs were selected to derive the volume of interest (VOI). Then texture parameters values based on ADC map were calculated automatically. Three kinds of parameters were generated automatically, including histogram, the gray-level co-occurrence matrix (GLCM), and the gray level run length matrix (GLRLM). In this study, we evaluated 7 texture parameters, which were divided 2 groups: first-order from histogram and second-order from GLCM. Skewness, kurtosis, and uniformity from the histogram parameters were used in this study. They have been studied previously and have been proven to be related to lesion heterogeneity [21–23]. Entropy, energy, inertia, and correlation, which derived from the basic GLCM, are also well studied, which describe the relationship between adjacent pixels in the region of interest, as described in Table 2.

Potential Prognostic Factors

Prognostic factors in clinical and histopathology were reviewed from the clinical database. Plasma CEA level (ng/ml) was evaluated using our institution's CEA threshold. Microscopic histopathological analysis of specimens was performed by the pathologist (Mei Wu, with 10 years of experience in gastrointestinal pathology). pT stage (pT1-T4) and pN

Table 1 MRI sequences for rectal imaging

MRI sequence	TR(ms)	TE (ms)	FSE factor	Slice thickness(mm)	Gap(mm)	FOV(cm)	Matrix	NSA	b-value
Sagittal T_2WI	3577	70	20	3	0	24x24x7.2	300 × 266	3	–
Coronal T_2WI	3000	75	18	2	0	18x18x0.4	300 × 218	3	–
Axial T_2WI	3000	75	18	3	0	18x18x7.2	368 × 273	3	–
Axial DWI	2750	76	–	3	0	22x22x7.2	112 × 108	2	0, 1000

TR: repetition time; TE: echo time; FSE: fast spin echo; FOV: field of view; NSA: number of signal averaged

stage (pN0-N2) were evaluated according to the American Joint Committee on Cancer (AJCC) 7th edition staging manual [24]. Tumors are classified as grade 1, grade 2, and grade 3 when gland-like structures in the tumor occupy greater than 95%, greater than 50% but less than or equal to 95%, or less than or equal to 50% of the volume, respectively, according to WHO grading criteria [25]. Grade 1 and grade 2 were appointed as low-grade tumors and grade 3 was appointed as high-grade tumors. CRM, peritumor LVI or neural invasion were reported as negative or positive.

Statistical Analysis

All texture parameters were firstly tested by Kolmogorov–Smirnov test for normality analysis. Independent sample *t*-test or Mann-Whitney *U*-test were used to analyze and compare the differences between all texture parameters of the following: (1) CEA ≤ 7.0 ng/ml and > 7.0 ng/ml, (2) pT1–2 and pT3–4, (3) pN0 and pN1–2, (4) grade 1–2 and grade 3, (5) LVI or neural invasion showing negative and positive, (6) CRM showing negative and positive.

Binary logistic regression analysis with statistically significant texture parameters was used to identify logistic parameters for clinical and histological prognostic factors. A receiver operating characteristic (ROC) analysis was used to assess the diagnostic utility of statistically significant texture parameters and logistic parameter for the detection of high-stage tumors. The areas under curves (AUCs) were compared using the method of Delong et al. [26]. The interobserver agreement of texture parameters was evaluated by using the following intra-class correlation (ICC) coefficient test: 0.00–0.20, poor agreement; 0.21–0.40, fair agreement; 0.41–0.60, moderate agreement; 0.61–0.80, good agreement; 0.81–1.00, excellent agreement. Statistical analysis was performed using SPSS software (SPSS, version 16.0; SPSS, Chicago, IL, USA) and MedCalc software (MedCalc, version 9.0; MedCalc Software, Mariakierke, Belgium). The level of statistical significance was set at $P \leq 0.05$.

Table 2 Detailed description of texture parameters

Texture parameters	Description
Skewness	Reflects asymmetry of the pixel distribution
Kurtosis	Reflects peakedness and tailedness of the histogram
Uniformity	Reflects randomness of the pixel distribution
Entropy	Reflects disorder of gray-level distribution
Energy	Reflects the average of the gray level co-occurrences
Inertia	Reflects variation in signal intensities
Correlation	Reflects the linear dependencies of gray levels

Results

Clinical and Histopathological Findings

A summary of the prognostic factor distribution in our study is given in Table 3. In brief, 59 patients had CEA levels less than or equal to 7 ng/ml. The remaining 41 patients had CEA levels greater than 7 ng/ml. According to the histopathological analysis, 38 tumors were limited to the rectal muscularis propria (8 tumors were pT1, 30 tumors were pT2), while the remaining 62 tumors extended beyond the muscularis propria (57 tumors were pT3 and 5 tumors were pT4). Fifty-six patients were staged as N0, 29 patients were staged as N1, and the remaining 15 patients as N2. Based on WHO grading criteria, 58 tumors were classified as grade 2, and 42 tumors were classified as grade 3. However, no tumors were classified as grade 1. Among the patients, CRM was positive in 19 patients, and peritumor LVI or neural invasion were positive in 10 patients.

Interobserver Agreement

All texture parameters derived from ADC maps delineated separately by two radiologists showed excellent agreement (ICCs ranged from 0.887 to 0.953).

Texture Parameters among Prognostic Factors

The differences in texture parameters within each group of prognostic factors are shown in Table 3. In the pT stage group, uniformity, energy and entropy were significantly different

Table 3 Texture parameters for different prognostic factors' groups of rectal cancer

Prognostic factor	n	Skewness[a]	Kurtosis[a]	Uniformity[b]	Energy ($\times 10^{-3}$)[b]	Entropy[a]	Inertia[a]	Correlation ($\times 10^{-3}$)[b]
CEA level								
≤ 7 ng/ml	59	0.348 ± 0.37	0.711 ± 0.76	0.783 ± 0.06	0.925 ± 1.22	10.064 ± 1.17	960.829 ± 551.55	0.487 ± 0.37
> 7 ng/ml	41	0.357 ± 0.29	0.429 ± 0.63	0.778 ± 0.08	0.802 ± 0.93	9.930 ± 1.37	1104.516 ± 735.92	0.425 ± 0.23
p value		0.907	0.053	0.602	0.777	0.602	0.267	0.158
pT stage								
pT1–2	38	0.377 ± 0.35	0.528 ± 0.72	0.790 ± 0.06	1.297 ± 1.55	9.572 ± 1.23	1141.925 ± 704.87	0.461 ± 0.25
pT3–4	62	0.336 ± 0.34	0.636 ± 0.72	0.775 ± 0.09	0.713 ± 0.85	10.277 ± 1.20	944.853 ± 579.83	0.481 ± 0.32
p value		0.565	0.470	**0.026**	**0.001**	**0.006**	0.132	0.329
pN stage								
pN0	56	0.405 ± 0.35	0.580 ± 0.78	0.785 ± 0.06	0.893 ± 1.05	10.079 ± 1.15	993.943 ± 626.26	0.487 ± 0.41
pN1–2	44	0.284 ± 0.32	0.614 ± 0.63	0.778 ± 0.09	0.797 ± 1.48	9.921 ± 1.39	1052.574 ± 649.71	0.462 ± 0.27
p value		0.075	0.811	0.268	0.981	0.535	0.649	0.231
Grade								
Grade 1–2	58	0.186 ± 0.27	0.429 ± 0.72	0.785 ± 0.06	0.991 ± 1.35	9.845 ± 1.22	1123.45 ± 679.60	0.480 ± 0.41
Grade 3	42	0.581 ± 0.29	0.824 ± 0.65	0.774 ± 0.09	0.736 ± 0.84	10.236 ± 1.27	876.52 ± 540.90	0.447 ± 0.22
p value		**0.000**	**0.006**	0.178	0.061	0.124	0.054	**0.041**
CRM								
Negative	81	0.354 ± 0.33	0.551 ± 0.74	0.783 ± 0.06	0.972 ± 1.20	9.880 ± 1.27	1073.787 ± 669.46	0.475 ± 0.33
Positive	19	0.344 ± 0.38	0.783 ± 0.57	0.777 ± 0.08	0.667 ± 0.59	10.560 ± 1.04	789.331 ± 387.84	0.476 ± 0.29
p value		0.911	0.205	0.638	**0.008**	**0.033**	0.078	0.632
LVI or neural invasion								
Negative	90	0.370 ± 0.34	0.612 ± 0.71	0.778 ± 0.07	0.872 ± 1.07	9.973 ± 1.26	1027.813 ± 653.37	0.487 ± 0.32
Positive	10	0.186 ± 0.29	0.440 ± 0.82	0.794 ± 0.06	0.735 ± 1.58	10.336 ± 1.23	947.092 ± 441.60	0.399 ± 0.21
p value		0.105	0.475	0.175	0.558	0.387	0.705	0.095

[a] Independent sample t-test, normally distributed data are mean ± standard deviation;

[b] Mann-Whitney U-test, non-normal data are median ± interquartile range

($p = 0.026$, 0.001, and 0.006 respectively) between stage pT1–2 and pT3–4 tumors. Specifically, uniformity and energy were higher in pT1–2 stage than in pT3–4 stage, while entropy was lower in pT1–2 stage than in pT3–4 stage. In the grade group, skewness and kurtosis were significant lower ($p = 0.000$ and 0.006 respectively) in grade 1–2 than in grade 3 tumors, while correlation was significant higher ($p = 0.041$) in grade 1–2 than in grade 3 tumors. In the CRM group, energy was significant higher ($p = 0.008$) for negative CRM than for positive CRM, while entropy was significant lower ($p = 0.033$) for negative CRM than for positive CRM. No significant inter-group differences were observed with respect to CEA level (≤ 7.0 and > 7.0 ng/ml), pN stage (pN0 and pN1–2) and LVI or neural invasion (negative and positive).

Diagnostic Performance of Texture Parameters

Table 4 shows the diagnostic performance of statistically significant texture features and logistic parameters using ROC analysis to discriminate high-stage tumors. For differentiating pT3-T4 stage tumors from pT1-T2 stage tumors, the AUCs of uniformity, energy and entropy were 0.633, 0.695, and 0.681 respectively. Using a logistic regression model that incorporated those three texture parameters, we achieved moderate accuracy (AUC, 0.723) with a sensitivity of 56.5% and specificity of 84.2% (Fig. 1). There are no significant differences in AUC between any two texture parameters. For differentiating grade 3 from grade 1–2 tumors, the AUCs of skewness, kurtosis, and correlation were 0.854, 0.672, and 0.620 respectively. Using a logistic regression model that incorporated those three texture parameters, we achieved a high accuracy (AUC, 0.904) with a sensitivity of 81.0% and specificity of 87.9% (Fig. 2). The AUC for logistic parameter was significantly higher than the AUC for skewness, kurtosis and correlation ($p = 0.0354$, <0.0001 and <0.0001 respectively). For differentiating positive from negative of CRM, the AUCs of energy and entropy were 0.696 and 0.654 respectively. Using a logistic regression model that incorporated those two texture parameters, the accuracy was similar with energy (Fig. 3). There were no significant differences in AUC between any two texture parameters.

Table 4 Diagnostic performance of statistically significant texture parameters and logistic parameter to discriminate high-stage tumors

Parameter	Cutoff value	AUC (95% CI)	Sensitivity	Specificity	Comparison of AUC (*p* value)			
T stage					uniformity	energy	entropy	logistic parameter
Uniformity	≤ 0.7168	0.633 (0.531, 0.728)	25.8%	97.4%	–	0.3569	0.4859	0.0550
Energy	$\leq 9.377 \times 10^{-3}$	0.695 (0.595, 0.783)	56.5%	84.2%		–	0.3041	0.4425
Entropy	> 6.9945	0.681 (0.580, 0.771)	59.7%	78.9%			–	0.2323
Logistic parameter	> -0.3015	0.723 (0.625, 0.808)	56.5%	84.2%				–
Grade					skewness	kurtosis	correlation	logistic parameter
Skewness	> 0.429	0.854 (0.770, 0.917)	81.0%	79.3%	–	0.0016	0.0029	0.0354
Kurtosis	> 0.7112	0.672 (0.571, 0.763)	59.5%	70.7%		–	0.5442	<0.0001
Correlation	$\leq 0.644 \times 10^{-3}$	0.620 (0.517, 0.715)	90.5%	36.2%			–	<0.0001
Logistic parameter	> 0.0025	0.904 (0.829, 0.954)	81.0%	87.9%				–
CRM						energy	entropy	logistic parameter
Energy	$\leq 0.7436 \times 10^{-3}$	0.696 (0.568, 0.823)	68.4%	63.0%		–	0.2948	0.8164
Entropy	> 10.003	0.654 (0.552, 0.746)	78.9%	49.4%			–	0.2901
Logistic parameter	≤ 0.5184	0.696 (0.569, 0.823)	68.4%	63.0%				–

Discussion

In this study, we found that uniformity, energy and entropy could significantly differentiate stage pT1-pT2 tumors from stage pT3-pT4 tumors; skewness, kurtosis, and correlation could significantly differentiate grade 1–2 from grade 3 tumors; and energy and entropy could significantly differentiate negative CRM from positive CRM. Furthermore, we used a logistic regression model that incorporated statistically significant texture parameters. We found that logistic regression analysis predicted higher AUC for differentiating pT3–4 stage from pT1-pT2 and for differentiating grade 3 from grade 1–2 tumors, but not for differentiating positive CRM from negative CRM. The results indicate that texture features derived from ADC map are potentially valuable tools for predicting important histopathologic factors of rectal cancer.

Tumors in advanced rectal cancer are large, deeply infiltrated, and have greater cellularity, angiogenesis, extracellular matrix, necrosis, and hemorrhage. As a result, ADC maps in advanced stages of rectal cancer are more heterogeneous than in earlier stages. In the present study, we found that uniformity and energy were significantly higher in pT1–2 stage than in pT3–4 stage, while entropy was significantly lower in pT1–2 stage than in pT3–4 stage. Theoretically, uniformity and energy reflect how close the image is to a uniform distribution of gray levels [27]. Higher uniformity and energy indicate uniformity in image and lower heterogeneity [27, 28]. Entropy represents the spatial disorder of ADC gray-level distribution. A higher value for entropy reflects greater heterogeneity of the lesion [29]. These are key concepts for interpreting our findings. Similar results have been reported in other studies. Wibmer et al. [18] demonstrated that prostate cancers showed lower energy compared to non-cancerous prostate on ADC maps. Our finding that entropy can differentiate pT1–2 from pT3–4 stage rectal cancer was similar to findings in the studies by Liu et al. [30] and Li et al. [31]. In our study, logistic regression analysis was used for probability predictions. The AUC of predicted probability derived by logistic regression analysis was more favorable than three statistically significant texture parameters; this finding was consistent with the study by Liu et al. [30].

Histologic grade is the significant clinical factor for recurrence and survival in rectal cancer patients [32]. The histologic grade is determined by the proportion of glandular formation

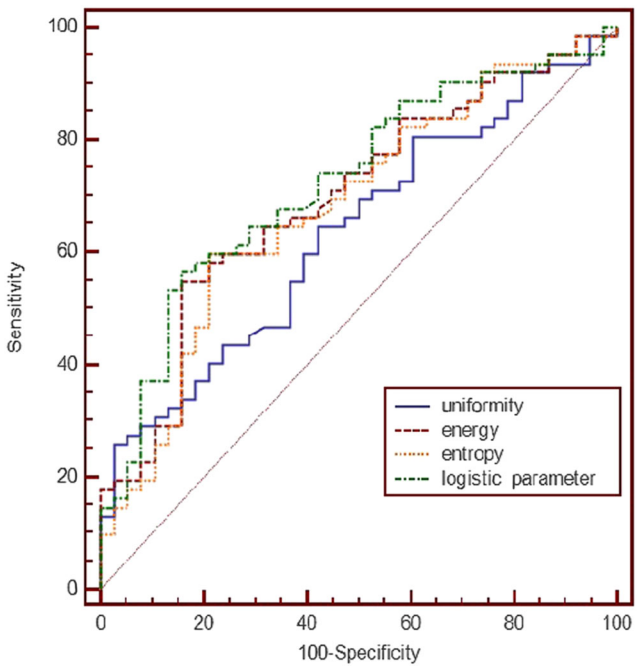

Fig. 1 ROC curves are shown analyzing the discriminatory power to differentiate stage pT1–2 and pT3–4 tumors. The corresponding AUCs are listed in Table 4

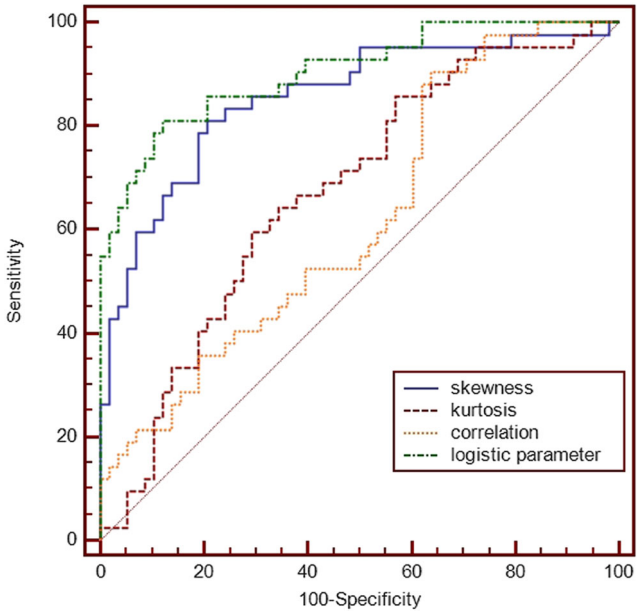

Fig. 2 ROC curves are shown analyzing the discriminatory power to differentiate grade G1–2 and G3 tumors. The corresponding AUCs are listed in Table 4

in the tumor [32]. High-grade tumors have less than or equal to 50% glandular formation. As a result, high-grade tumors manifest marked atypia, a large nuclear volume fraction, increased cell density, and micronecrosis [33]. Therefore, the microstructures in high-grade tumors are more complex and heterogeneous than those in the low-grade tumors. In our study, skewness, kurtosis were significant lower in low-grade tumors than in high-grade tumors, while correlation was significant higher in low-grade tumors than in high-grade tumors. Skewness reflects asymmetry of the pixel distribution. Positively skewness means the distribution of the histogram has an elongated tail on the right side of the mean [13]. Kurtosis reflects the peakedness of the distribution and is a measure of the shape of the probability distribution [13]. Higher values for skewness and kurtosis represent greater complexity and heterogeneity in tumors. Correlation is a measure of the linear dependencies of gray levels. Higher values for correlation represent less heterogeneity in tumors. Skewness, kurtosis and correlation may therefore be useful as imaging biomarkers for differentiating between histologic grades of rectal cancer. Others have reported similar findings. Rozenberg et al. [34] reported that skewness and kurtosis were promising predictors for Gleason Score (GS) upgrading among GS 3 + 4 = 7 tumors and for differentiating between intermediate-risk cancers. In the study by Meng et al. [35], correlations showed significant differences between patients with different prognoses. We have demonstrated that a logistic regression model that factored skewness, kurtosis and correlation improved diagnostic efficacy for predicting the histologic grade of rectal cancer.

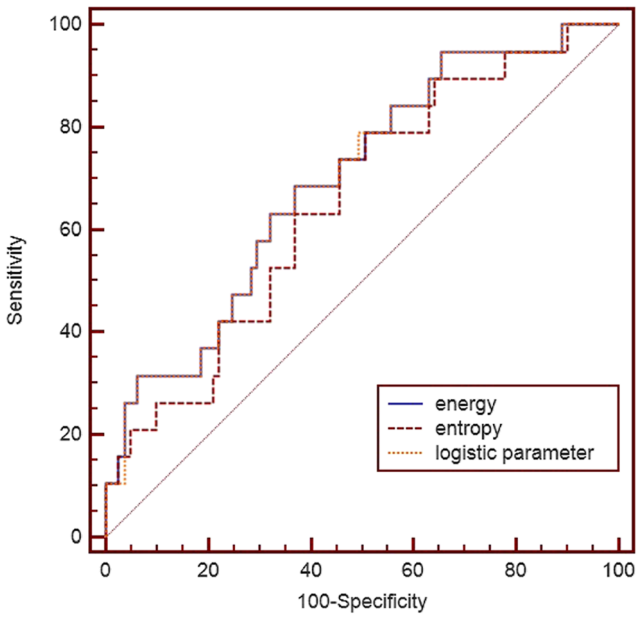

Fig. 3 ROC curves are shown analyzing the discriminatory power to differentiate negative and positive CRM. The corresponding AUCs are listed in Table 4

CRM is positive if there is less than 1 mm between the tumor and the CRM at histopathologic examination. Positive CRM is an important predisposing factor for local recurrence [36]. Tumors with positive CRM have large volume and have more cellularity, angiogenesis, extracellular matrix, necrosis, and hemorrhage. As a result, ADC maps for tumors of positive CRM have greater heterogeneity compared with negative CRM. In our study, the tumor of positive CRM had significantly lower energy and higher entropy than negative CRM, which was consistent with the theoretical description of energy and entropy. Previous studies [37, 38] had reported that mean ADC value derived from an ADC map could not significantly differentiate between negative and positive CRM. Moreover, Cui et al. [39] demonstrated that no significant differences were found for ADC first-order texture features (histogram metrics) in the status of CRM. So, our result demonstrated that energy and entropy might be useful as imaging biomarkers for predicting CRM involvement.

Nodal involvement may be an indication for preoperative neoadjuvant chemotherapy and radiation therapy. In the present study, no significant differences were found for all texture parameters in tumors at pN stage. Our findings were in accord with the study of Li et al. [31] . However, our findings were in conflict with the study of Liu et al. [30], which demonstrated that significant differences in entropy between pN0 and pN1–2 tumors. The contradiction may be attributed to the DWI parameters. In the study of Liu et al. [30], slice thickness was 5–7 mm and slice gap was 10% of slice thickness. In the present study, slice thickness was 3 mm and slice gap was 0 mm. In the study of Li et al. [31], the slice thickness and slice gap were similar to our study. The segmentation of regions of lesions was approximately whole tumor in our

study and in the study by Li et al. [31] . It was previously reported that CEA may be another important prognostic factor of rectal cancer [2] **.** However, our findings showed no correlation between texture features and CEA levels. Therefore, we think that the CEA level might not reflect the actual status of the rectal cancer at the time of diagnosis. In addition, our findings showed no correlation between texture features and LVI or neural involvement. It seemed that positive LVI or neural involvement did not induce significant changes in microstructures of tumors. Similar findings have also been reported by Li et al. [31].

However, this study has a few limitations. First, a retrospective analysis such as ours inevitably incurs selection bias. Second, rectal cancer usually grows along the rectal wall and forms an irregular shape. In addition, intestinal gas causes artifacts and distortion on DWI. So, the VOI of consecutive sections may not accurately represent the actual whole tumor volume. Third, according to previous studies [40, 41], the extramural depth of tumor invasion is an independent prognostic factor in patients with pT3 rectal cancer. The prognosis of pT3a (extramural depth <5 mm) is similar to the prognosis of pT2 rectal cancer. The pT3 subclassification stage was not included in this study, but could be investigated in future studies. Finally, histogram-derived as well as GLCM-derived texture features from DWI datasets are sensitive to the applied b-values [42] . We only analyzed one ADC map. In future studies, the choice of the b-value need to be taken into account.

Conclusions

In conclusion, texture features derived from ADC maps may be useful for predicting important histopathologic factors in rectal cancer. In particular, uniformity, energy and entropy have the potential to differentiate among stages of rectal cancer; skewness, kurtosis, and correlation have the potential to differentiate histologic high-grade tumor; and energy and entropy have the potential to predict CRM involvement.

Funding This study was funded by Jiangsu Provincial Medical Youth Talent (QNRC2016212), Suzhou Clinical Special Disease Diagnosis and Treatment Program (LCZX201823), Suzhou GuSu Medical Talent Project (GSWS2019077) and Science and Technology Bureau of Changshu (CS201624).

Compliance with Ethical Standards

Conflict of Interest Author Zhihua Lu has received research grants from Jiangsu Provincial Medical Youth Talent, Suzhou Clinical Special Disease Diagnosis and Treatment Program, Suzhou GuSu Medical Talent Project and Science and Technology Bureau of Changshu. Author Jianlong Jiang has received research grant from Suzhou Clinical Special Disease Diagnosis and Treatment Program. All authors have no relevant conflicts of interest including specific financial interests relevant to the subject of our manuscript.

Ethical Approval All procedures performed in studies involving human participants were in accordance with the ethical standards of the Institutional Review Board of Changshu Hospital Affiliated to Soochow University. Requirements for written informed consent were waived due to the retrospective nature of the study.

References

1. Schmoll, H. J., Van Cutsem, E., Stein, A., Valentini, V., Glimelius, B., Haustermans, K. et al., ESMO consensus guidelines for management of patients with colon and rectal cancer. A personalized approach to clinical decision making. Ann Oncol 23:2479–2516, 2012. https://doi.org/10.1093/annonc/mds236.
2. Boras, Z., Kondza, G., Sisljagić, V., Busić, Z., Gmajnić, R., and Istvanić, T., Prognostic factors of local recurrence and survival after curative rectal cancer surgery: A single institution experience. Coll Antropol 36:1355–1361, 2012.
3. Brown, G., Radcliffe, A. G., Newcombe, R. G., Dallimore, N. S., Bourne, M. W., and Williams, G. T., Preoperative assessment of prognostic factors in rectal cancer using high-resolution magnetic resonance imaging. Br J Surg 90:355–364, 2003. https://doi.org/10.1002/bjs.4034.
4. Lee, E. S., Kim, M. J., Park, S. C., Hur, B. Y., Hyun, J. H., Chang, H. J., Baek, J. Y., Kim, S. Y., Kim, D. Y., and Oh, J. H., Magnetic resonance imaging-detected extramural venous invasion in rectal Cancer before and after preoperative Chemoradiotherapy: Diagnostic performance and prognostic significance. Eur Radiol 28:496–505, 2018. https://doi.org/10.1007/s00330-017-4978-6.
5. Cienfuegos, J. A., Rotellar, F., Baixauli, J., Beorlegui, C., Sola, J. J., Arbea, L., Pastor, C., Arredondo, J., and Hernández-Lizoáin, J. L., Impact of perineural and lymphovascular invasion on oncological outcomes in rectal cancer treated with neoadjuvant chemoradiotherapy and surgery. Ann Surg Oncol 22:916–923, 2015. https://doi.org/10.1245/s10434-014-4051-5.
6. Bammer, R., Basic principles of diffusion-weighted imaging. Eur J Radiol 45:169–184, 2003. https://doi.org/10.1016/S0720-048X(02)00303-0.
7. Padhani, A. R., Liu, G., Koh, D. M., Chenevert, T. L., Thoeny, H. C., Takahara, T. et al., Diffusion-weighted magnetic resonance imaging as a cancer biomarker: Consensus and recommendations. Neoplasia 11:102–125, 2009.
8. Curvo-Semedo, L., Lambregts, D. M., Maas, M., Beets, G. L., Caseiro-Alves, F., and Beets-Tan, R. G., Diffusion-weighted MRI in rectal cancer: Apparent diffusion coefficient as a potential noninvasive marker of tumor aggressiveness. J Magn Reson Imaging 35:1365–1371, 2012. https://doi.org/10.1002/jmri.23589.
9. Attenberger, U. I., Pilz, L. R., Morelli, J. N., Hausmann, D., Doyon, F., Hofheinz, R., Kienle, P., Post, S., Michaely, H. J., Schoenberg, S. O., and Dinter, D. J., Multi-parametric MRI of rectal cancer - do quantitative functional MR measurements correlate with radiologic and pathologic tumor stages? Eur J Radiol 83:1036–1043, 2014. https://doi.org/10.1016/j.ejrad.2014.03.012.
10. Oh, J. W., Rha, S. E., Oh, S. N., Park, M. Y., Byun, J. Y., and Lee, A., Diffusion-weighted MRI of epithelial ovarian cancers: Correlation of apparent diffusion coefficient values with histologic grade and surgical stage. Eur J Radiol 84:590–595, 2015. https://doi.org/10.1016/j.ejrad.2015.01.005.
11. Hecht, E. M., Liu, M. Z., Prince, M. R., Jambawalikar, S., Remotti, H. E., Weisberg, S. W., Garmon, D., Lopez-Pintado, S., Woo, Y., Kluger, M. D., and Chabot, J. A., Can diffusion-weighted imaging

serve as a biomarker of fibrosis in pancreatic adenocarcinoma? J Magn Reson Imaging 46:393–402, 2017. https://doi.org/10.1002/jmri.25581.

12. Barnes, S. L., Sorace, A. G., Whisenant, J. G., McIntyre, J. O., Kang, H., and Yankeelov, T. E., DCE- and DW-MRI as early imaging biomarkers of treatment response in a preclinical model of triple negative breast cancer. NMR Biomed 30:e3799, 2017. https://doi.org/10.1002/nbm.3799.
13. Just, N., Improving tumor heterogeneity MRI assessment with histograms. Br J Cancer 111:2205–2213, 2014. https://doi.org/10.1038/bjc.2014.512.
14. Gillies, R. J., Kinahan, P. E., and Hricak, H., Radiomics: Images are more than pictures, they are data. Radiology 278:563–577, 2016. https://doi.org/10.1148/radiol.2015151169.
15. Becker, A. S., Ghafoor, S., Marcon, M., Perucho, J. A., Wurnig, M. C., Wagner, M. W., Khong, P. L., Lee, E. Y., and Boss, A., MRI texture features may predict differentiation and nodal stage of cervical cancer: A pilot study. Acta Radiol Open 6: 2058460117729574, 2017. https://doi.org/10.1177/2058460117729574.
16. Xia, K., Yin, H., Qian, P., Jiang, Y., and Wang, S., Liver semantic segmentation algorithm based on improved deep adversarial networks in combination of weighted loss function on abdominal CT images. IEEE Access 7:96349–96358, 2019.
17. Xia, K., Yin, H., and Zhang, Y., Deep semantic segmentation of kidney and space-occupying lesion area based on SCNN and ResNet models combined with SIFT-flow algorithm. J. Medical Systems 43:2:1–2:12, 2018. https://doi.org/10.1007/s10916-018-1116-1.
18. Wibmer, A., Hricak, H., Gondo, T., Matsumoto, K., Veeraraghavan, H., Fehr, D. et al., Haralick texture analysis of prostate MRI: Utility for differentiating non-cancerous prostate from prostate cancer and differentiating prostate cancers with different Gleason scores. Eur Radiol 25:2840–2850, 2015. https://doi.org/10.1007/s00330-015-3701-8.
19. Ytre-Hauge, S., Dybvik, J. A., Lundervold, A., Salvesen, Ø. O., Krakstad, C., Fasmer, K. E. et al., Preoperative tumor texture analysis on MRI predicts high-risk disease and reduced survival in endometrial cancer. J Magn Reson Imaging 48:1637–1647, 2018. https://doi.org/10.1002/jmri.26184.
20. Ueno, Y., Forghani, B., Forghani, R., Dohan, A., Zeng, X. Z., Chamming's, F., Arseneau, J., Fu, L., Gilbert, L., Gallix, B., and Reinhold, C., Endometrial carcinoma: MR imaging-based texture model for preoperative risk stratification-a preliminary analysis. Radiology 284:748–757, 2017. https://doi.org/10.1148/radiol.2017161950.
21. Kyriazi, S., Collins, D. J., Messiou, C., Pennert, K., Davidson, R. L., Giles, S. L., Kaye, S. B., and Desouza, N. M., Metastatic ovarian and primary peritoneal cancer: Assessing chemotherapy response with diffusion-weighted MR imaging–value of histogram analysis of apparent diffusion coefficients. Radiology 261:182–192, 2011. https://doi.org/10.1148/radiol.11110577.
22. Choi, M. H., Oh, S. N., Rha, S. E., Choi, J. I., Lee, S. H., Jang, H. S., Kim, J. G., Grimm, R., and Son, Y., Diffusion-weighted imaging: Apparent diffusion coefficient histogram analysis for detecting pathologic complete response to chemoradiotherapy in locally advanced rectal cancer. J Magn Reson Imaging 44:212–220, 2016. https://doi.org/10.1002/jmri.25117.
23. Meng, Y., Zhang, C., Zou, S., Zhao, X., Xu, K., Zhang, H., and Zhou, C., MRI texture analysis in predicting treatment response to neoadjuvant chemoradiotherapy in rectal cancer. Oncotarget 9: 11999–12008, 2017. https://doi.org/10.18632/oncotarget.23813.
24. Edge SB, Byrd DR, Compton CC (2010) American Joint Committee on Cancer. AJCC cancer staging manual. 7th ed. Springer, New York
25. Bosman, F. T., Carneiro, F., and Hruban, R. H., WHO classification of tumors of the digestive system. Geneva: World Health Organization, 2010.
26. DeLong, E. R., DeLong, D. M., and Clarke-Pearson, D. L., Comparing the areas under two or more correlated receiver operating characteristic curves: A nonparametric approach. Biometrics 44:837–845, 1988.
27. Kim, J. H., Ko, E. S., Lim, Y., Lee, K. S., Han, B. K., Ko, E. Y., Hahn, S. Y., and Nam, S. J., Breast Cancer heterogeneity: MR imaging texture analysis and survival outcomes. Radiology 282: 665–675, 2017. https://doi.org/10.1148/radiol.2016160261.
28. Caruso, D., Zerunian, M., Ciolina, M., de Santis, D., Rengo, M., Soomro, M. H. et al., Haralick's texture features for the prediction of response to therapy in colorectal cancer: A preliminary study. Radiol Med 123:161–167, 2018. https://doi.org/10.1007/s11547-017-0833-8.
29. Duvauferrier, R., Bezy, J., Bertaud, V., Toussaint, G., Morelli, J., and Lasbleiz, J., Texture analysis software: Integration with a radiological workstation. Stud Health Technol Inform 180:1030–1034, 2012.
30. Liu, L., Liu, Y., Xu, L., Li, Z., Lv, H., Dong, N., Li, W., Yang, Z., Wang, Z., and Jin, E., Application of texture analysis based on apparent diffusion coefficient maps in discriminating different stages of rectal cancer. J Magn Reson Imaging 45:1798–1808, 2017. https://doi.org/10.1002/jmri.25460.
31. Li, W., Jiang, Z., Guan, Y., Chen, Y., Huang, X., Liu, S., He, J., Zhou, Z., and Ge, Y., Whole-lesion apparent diffusion coefficient first- and second-order texture features for the characterization of rectal Cancer pathological factors. J Comput Assist Tomogr 42: 642–647, 2018. https://doi.org/10.1097/RCT.0000000000000731.
32. Song, J. H., Kim, S. H., Lee, J. H., Cho, H. M., Kim, D. Y., Kim, T. H. et al., Significance of histologic tumor grade in rectal cancer treated with preoperative chemoradiotherapy followed by curative surgery: A multi-institutional retrospective study. Radiother Oncol 118:387–392, 2016. https://doi.org/10.1016/j.radonc.2015.11.028.
33. Zhu, L., Pan, Z., Ma, Q., Yang, W., Shi, H., Fu, C., Yan, X., Du, L., Yan, F., and Zhang, H., Diffusion kurtosis imaging study of rectal adenocarcinoma associated with Histopathologic prognostic factors: Preliminary findings. Radiology 284:66–76, 2017. https://doi.org/10.1148/radiol.2016160094.
34. Rozenberg, R., Thornhill, R. E., Flood, T. A., Hakim, S. W., Lim, C., and Schieda, N., Whole-tumor quantitative apparent diffusion coefficient histogram and texture analysis to predict Gleason score upgrading in intermediate-risk 3 + 4 = 7 prostate Cancer. AJR Am J Roentgenol 206:775–782, 2016. https://doi.org/10.2214/AJR.15.15462.
35. Meng, J., Zhu, L., Zhu, L., Xie, L., Wang, H., Liu, S. et al., Whole-lesion ADC histogram and texture analysis in predicting recurrence of cervical cancer treated with CCRT. Oncotarget 8:92442–92453, 2017. https://doi.org/10.18632/oncotarget.21374.
36. Kaur, H., Choi, H., You, Y. N., Rauch, G. M., Jensen, C. T., Hou, P., Chang, G. J., Skibber, J. M., and Ernst, R. D., MR imaging for preoperative evaluation of primary rectal cancer: Practical considerations. Radiographics 32:389–409, 2012. https://doi.org/10.1148/rg.322115122.
37. Akashi, M., Nakahusa, Y., Yakabe, T., Egashira, Y., Koga, Y., Sumi, K., Noshiro, H., Irie, H., Tokunaga, O., and Miyazaki, K., Assessment of aggressiveness of rectal cancer using 3-T MRI: Correlation between the apparent diffusion coefficient as a potential imaging biomarker and histologic prognostic factors. Acta Radiol 55:524–531, 2013. https://doi.org/10.1177/0284185113503154.
38. Sun, Y., Tong, T., Cai, S., Bi, R., Xin, C., and Gu, Y., Apparent diffusion coefficient (ADC) value: A potential imaging biomarker that reflects the biological features of rectal cancer. PLoS One 9: e109371, 2014. https://doi.org/10.1371/journal.pone.0109371.

39. Cui, Y., Yang, X., Du, X., Zhuo, Z., Xin, L., and Cheng, X., Whole-tumor diffusion kurtosis MR imaging histogram analysis of rectal adenocarcinoma: Correlation with clinical pathologic prognostic factors. Eur Radiol 28:1485–1494, 2018. https://doi.org/10.1007/s00330-017-5094-3.
40. Merkel, S., Mansmann, U., Siassi, M., Papadopoulos, T., Hohenberger, W., and Hermanek, P., The prognostic inhomogeneity in pT3 rectal carcinomas. Int J Colorectal Dis 16:298–304, 2001.
41. Cho, S. H., Kim, S. H., Bae, J. H., Jang, Y. J., Kim, H. J., Lee, D., Park, J. S., and Society of North America (RSNA), Prognostic stratification by extramural depth of tumor invasion of primary rectal cancer based on the Radiological Society of North America proposal. AJR Am J Roentgenol 202:1238–1244, 2014. https://doi.org/10.2214/AJR.13.11311.
42. Becker, A. S., Wagner, M. W., Wurnig, M. C., and Boss, A., Diffusion-weighted imaging of the abdomen: Impact of b-values on texture analysis features. NMR Biomed 30:e3669, 2017. https://doi.org/10.1002/nbm.3669.